A Fully Integrated Surface Micromachined Magnetic Microactuator with a Multilevel Meander Magnetic Core

Chong H. Ahn, *Member, IEEE*, Mark G. Allen, *Member, IEEE*

Abstract—**A fully integrated magnetic microactuator using surface micromachining techniques is presented. To achieve this device, low-resistance meander conductors located in a single plane were interwoven with multilevel meander magnetic cores. This "wrapped" solenoid (with the core wrapped around the conductor) was fabricated in a fully integrated fashion. A magnetic microactuator was realized by incorporating a surface micromachined nickel–iron cantilever beam as part of the magnetic circuit of the core. The nickel–iron cantilever beam was 2.5 μm thick, 25 μm wide, and 780 μm long, and the magnetic circuit contained 17 turns of meander-type solenoid coils. Cantilever beam tip deflection of 6 μm in the vertical direction was achieved when a dc voltage less than 1 V (and resulting drive current of 800 mA) was applied to the coils. This fully integrated multilevel topology offers advantages in a variety of micromagnetic applications, where actuators can be fabricated on the same substrate with an integrated circuit and actuated with low voltages.**

I. Introduction

RECENTLY there has been much work towards realizing practical magnetic-based microactuators for a variety of applications. These efforts have used hybrid techniques either to place magnetic components onto integrated planar coils [1], [2], or to introduce external magnetic fields onto integrated high-permeability moving parts [3]. One reason that these approaches have been taken is the difficulty in fabricating three-dimensional solenoid-type coils using a planar fabrication process. In this work we describe a new "meander" actuator geometry which alleviates this problem and which is therefore particularly useful in the integrated fabrication of magnetic microactuators (MMA's) [4].

The major limitations in realization of MMA's arise from poor scaling, difficulty in fabrication, and relatively high resistive losses [5], leading to relatively low actuation efficiencies. However, the usefulness of MMA's also depends strongly on the application [1], [6]. For example, automotive applications may require much less actuation efficiency than implantable biomedical applications. In addition, MMA's may be an attractive microactuation scheme in cases, such as dust-filled environments, operation in conducting fluids, and operation in environments where high driving voltages are unacceptable or unattainable. Since magnetic actuators are current-controlled, they can in theory be operated even at low voltages, which can be obtained from conventional power sources without extra circuits for high voltage generation (of course, maximum current output and slew rate rather than maximum voltage output and slew rate become the controlling power supply issues). In addition, magnetic forces may be more suitable in long-range actuation [1], [6]. Finally, a micromagnetic structure can play a useful role as an electrical power generator [7] as well as a microactuator. These benefits of MMA's have motivated much of the current work in this field.

The requirements for an MMA are as follows. In order to produce a magnetic force (or actuation) at a specific location, magnetic microactuators should have an inductive component to generate magnetic flux, and a magnetic core to guide the generated flux to the point where actuation takes place. In addition, a fully integrated magnetic microactuator must satisfy additional material constraints; e.g., cores and moving parts must possess both high magnetic permeability and good mechanical properties. Some additional design constraints are: (1) mechanical structures such as cantilever beams, sliders, or magnetic rotors must be able to be inserted as a part of the magnetic circuit; (2) the length of the conductive coil wires should be short to minimize series resistance; (3) electromagnetic field interference (EMI) should be minimized, especially for actuators integrated with circuits; (4) the geometrical demagnetization effect should be minimized, such that an easy magnetic axis in the material can be readily produced; and (5) fully integrated fabrication should be possible. Methods for addressing most of these design constraints are discussed in the sections below.

Manuscript received October 26, 1992; revised April 8, 1993. Subject Editor, R. O. Warrington. This work was supported by the National Science Foundation under grant ECS-9117074.

The authors are with the School of Electrical Engineering, Microelectronics Research Center, Georgia Institute of Technology, Atlanta, GA 30332-0250.

IEEE Log Number 9209769.

II. Integrated Inductive Component Design

As mentioned above, an integrated MMA must have an inductive component flux generation. Several types of planar spiral inductive components with coils and magnetic material both in the same plane have been proposed

previously [8], [9], primarily because of ease of fabrication. However, the planar geometry alone does not satisfy the additional constraints for fully integrated MMA's described above. The flux generated from the spiral conductors will be spread out through the surface as both parallel and vertical components with respect to the surface [10]. As a result, it is not easy to guide flux to a required specific point unless a magnetic core is included as part of the inductor structure. In addition, the relatively long length of spiral conductors required for a large number of turns produces a high conductor resistance. Thus, investigation of alternative geometries for MMA realization is appropriate.

Consider the inductor geometries shown in Fig. 1. In the standard solenoid geometry shown in Fig. 1(b), a conductor line is "wrapped" around a magnetic core to form an inductive component. Such structures can be realized using multilevel metal interconnect schemes to "wrap" conductor lines around magnetic materials. These geometries are referred to in this paper as bar-type components, indicating that the magnetic core is in the shape of a solid bar. Geometries such as these have been used previously as the inductive component of magnetic sensors [11]. However, two potential problems arise from this geometry: first, the electrical via resistance from layer to layer may increase the total conductor resistance, depending on the fabrication process and the conductor material; second, the total conductor length must be relatively long. In addition, as relatively large currents may be flowing through these conductor coils, via reliability also becomes an issue. In spite of these problems, the bar-type geometry may be useful as a basic inductive component for magnetic microactuators if techniques are used to reduce the resistance of the via contacts.

Note that the same wrapping effect can be realized by switching the roles of conductor and core as in Fig. 1(a); imagine "wrapping" a magnetic core around a planar conductor line. This geometry can also be realized using multilevel metal interconnect schemes, by interlacing a meander planar conductor with a multilevel meander magnetic core. This "meander-type" geometry has two advantages over the "bar-type" geometry. First, there are no electrical vias to add resistance to the conductor coil. Second, the magnetic core is produced on two levels, making it readily available for surface micromachining of movable core actuators. In addition, the coils and cores in this geometry are magnetically tightly linked. The major disadvantage of the meander geometry is that the total core length (and thus the magnetic reluctance of the core) is increased by 3–4% compared with the core length without vias. In spite of this disadvantage, the "meander-type" geometry is attractive because of ease of fabrication as discussed below.

What particular materials should be used in MMA's? Three choices must be made: materials for the conductor coils, for the insulators, and for the magnetic core. The major characteristic of the coils must be low resistance, so that the MMA's can be driven at reasonable voltages

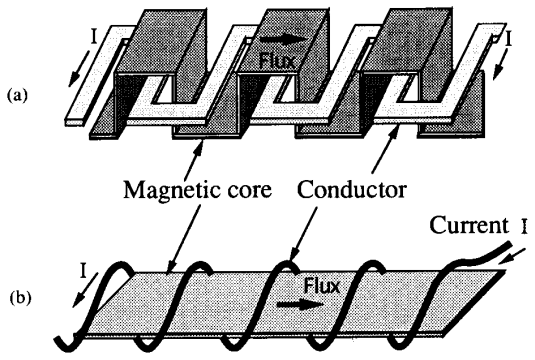

Fig. 1. Schematic diagram of a multilevel meander inductive component: (a) schematic diagram of meander-type as fabricated; (b) analogous structure illustrating the equivalence of 'wrapped' and meander type coils.

and currents without large coil power dissipation. This can be achieved by using a good conductor as the coil material, increasing the thickness of the conductor, and/or utilizing conductor geometries which minimize line length. Copper, gold, and aluminum have been used as conductor materials in previous MMA designs. In this research, both aluminum and copper were investigated as the conductor materials; gold conductors were not investigated because of the relatively higher cost involved in thick gold film deposition.

Insulators in MMA's satisfy both electrical and mechanical constraints. Consequently, the insulator should be a good dielectric material, and also should have good mechanical characteristics as a device molder or holder. To avoid mechanical distortion of microstructures embedded in insulators, low residual stress of the insulating material is required. In addition, its planarization ability plays a very important role in making possible a multilevel process. Polyimide, a good passivation organic material for integrated circuits, has good insulating properties as well as good planarization and mechanical properties.

The magnetic core in the MMA plays two roles: first, it is a mechanical component for actuation; second, it is a magnetic component for flux guidance. Nickel–iron Permalloy, in particular, displays outstanding characteristics as an MMA core material from the mechanical [12], magnetic [13], and processing viewpoints. Thus, these three materials were chosen for the magnetic microactuator.

In order to demonstrate the feasibility of flux generation using the meander geometry, a simple inductive structure without any actuator present was designed and fabricated [14]. A brief description of the fabrication procedure is provided here; full details can be found in [14] and are similar to those used to fabricated the MMA described later in this paper. The process starts with oxidized (0.6 μm) 2 in. ⟨100⟩ silicon wafers as a substrate. Onto this substrate, nickel (81%)–iron (19%) Permalloy was electroplated into the shape of the bottom core using patterned polyimide electroplating molds. A polyimide layer was

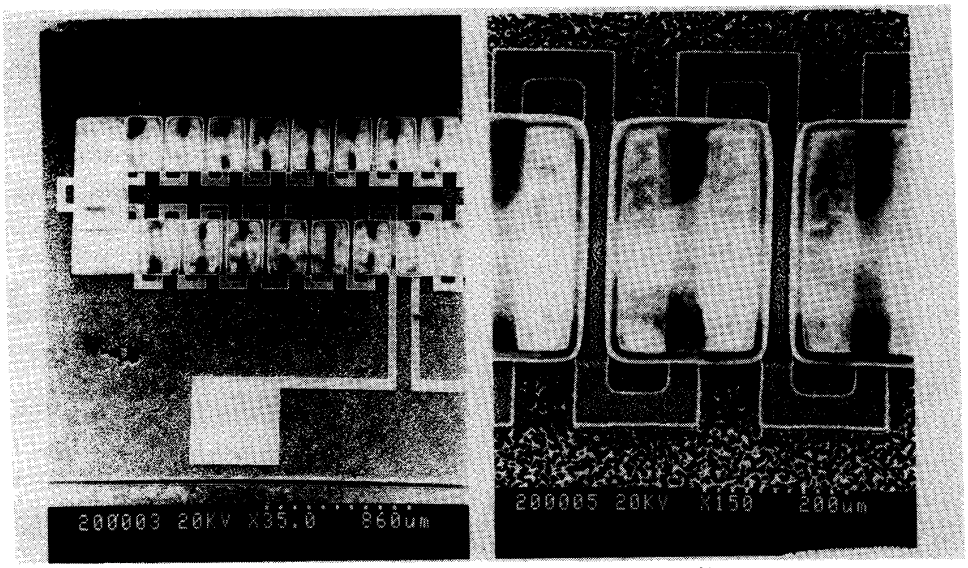

(a) (b)

Fig. 2. Scanning electron micrograph (SEM) of a fabricated multilevel meander inductor: (a) view showing half of the fabricated inductor structure; (b) detailed view of inductor elements.

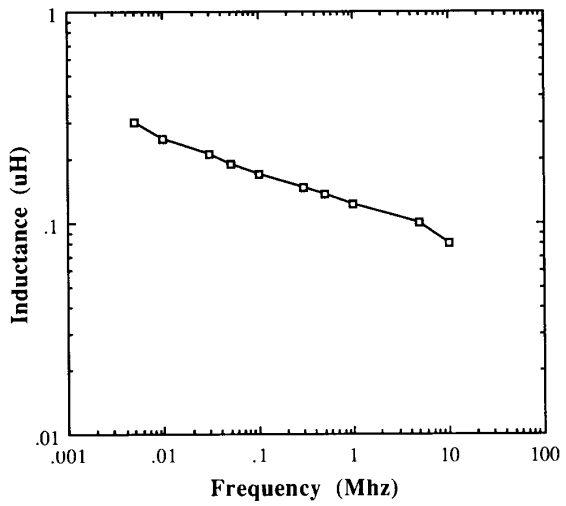

Fig. 3. The measured inductance of the fabricated multilevel meander inductive component.

then spin-coated onto the bottom cores, and the conductor coil was deposited and patterned. Additional polyimide was then deposited, and via holes were cut down through the polyimide to expose the bottom cores. These vias were filled using electroplated nickel (81%)-iron (19%) Permalloy, and the top magnetic cores (also Permalloy) were then deposited to complete the meander inductor.

Fig. 2 shows a scanning electron micrograph of the fabricated multilevel meander inductive component. The inductor structure has 26 turns with a size of 0.9 mm × 4 mm and a measured inductance of 0.2 μH at a test frequency of 100 kHz. The measured inductance of the meander inductive component as a function of frequency is shown in Fig. 3. It should be noted that even though there is a falloff in inductance as frequency is increased, most MMA's will be operated in the low-frequency regime, as the major limitation on bandwidth will come from the mechanical bandwidth of the actuator. Based on these results, the use of the meander geometry for MMA's was investigated.

III. Magnetic Microactuator Concept

By incorporating a surface micromachined nickel–iron cantilever beam as a part of the magnetic core, a fully integrated electromagnetic microactuator can be realized. Fig. 4(b) shows a schematic diagram of the MMA. Note that although the windings and cores are shown for the "bar-type" geometry in order to aid discussion, the actuator which will be designed and fabricated will be of the meander geometry described above.

The actuator works as follows. A current through the conductor coils causes flux to be generated in the core. The windings of the coils are such that the flux generated in both halves of the actuator will add in the center part. In the center part of the actuator, a cantilever beam of magnetic material is suspended over a base plate of magnetic material. The flux is thus forced through the air gap between the cantilever beam and the lower magnetic contact. A force of magnetic origin is thereby created that acts to reduce the total reluctance of the magnetic circuit by attracting the released cantilever beam toward the bottom magnetic contact.

Two advantages of the meander geometry in realizing this actuator should be reemphasized. First, owing to the multilevel core nature of the meander geometry, realizing the actuator and air gap is relatively easy. Second, in the fabrication of the actuator, electroplating will be used to

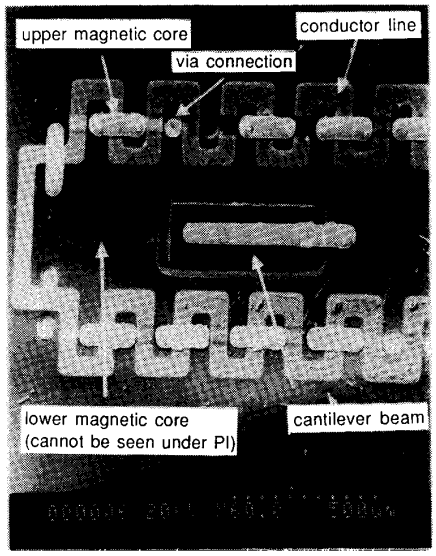

(a)

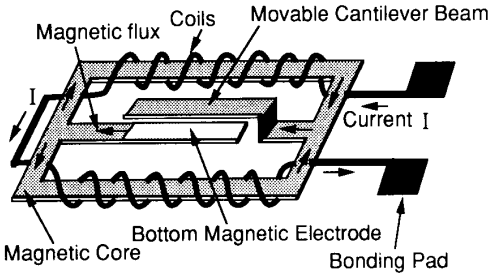

(b)

Fig. 4. Scanning electron micrograph (SEM) and schematic diagram of the integrated magnetic microactuator with nickel-iron cantilever beam. (a) Scanning electron micrograph (SEM): magnetic flux is guided both to the cantilever beam and to the bottom magnetic contact. Some upper magnetic core sections have been removed to show the magnetic vias. (b) Analogous schematic diagram: the actual meander type coil in the structure is represented as being equivalent to a "wrapped" solenoid type coil.

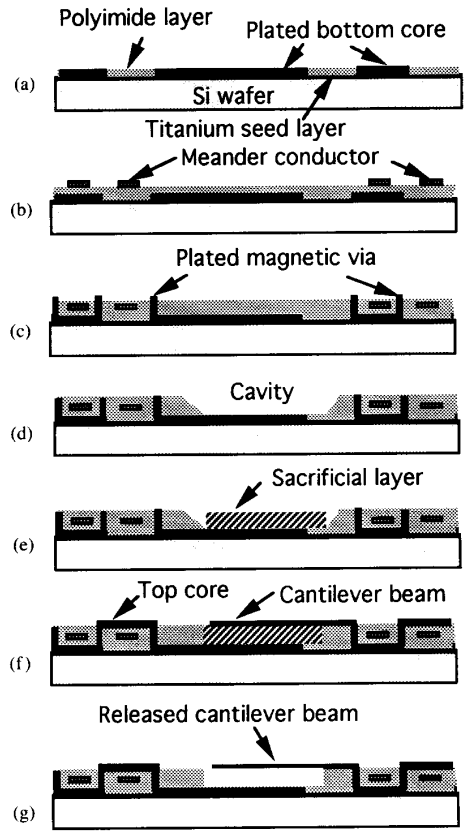

Fig. 5. Processing sequence to build a fully integrated magnetic microactuator. (a) Multi-spincoating of polyimide, dry etching, and bottom core plating; (b) patterning of conductor; (c) magnetic via plating; (d) dry etching of cavity; (e) patterning of sacrificial layer, (f) top core and cantilever beam plating; (g) release of cantilever beam.

realize relatively thick layers and to fill relatively deep via holes in the multilevel component. If a bar-type geometry is used, the multilevel component is the conductor. Thus, after fabrication of the conductor, it will be necessary to remove the seed layer, which is now at the bottom of a relatively complex structure. Although this can be done, it does result in much nonplanar processing, which is relatively difficult. However, if a meander geometry is used, the multilevel component is the magnetic core. As long as the electroplating seed layer is a nonmagnetic material, there is no need to remove it upon completion of the fabrication. Thus, almost all of the processing of the MMA can be done on relatively planar surfaces.

IV. Fabrication

A fabrication process summary of the MMA is given in Fig. 5, and is detailed below. The process started with oxidized (0.6 μm) 2 in. ⟨100⟩ silicon wafers as a substrate. Onto this substrate, an electroplating seed layer of titanium 2000 Å in thickness was deposited. Polyimide (Dupont PI-2611) was then spun on the wafer in three successive coats at 3000 rpm to build electroplating molds for the bottom magnetic core. The polyimide was cured at 350°C for 1 h in nitrogen, yielding an after-cure thickness of 9 μm. Holes were etched in this polyimide using a 4% CF_4/O_2 plasma etch and an aluminum hard mask until the titanium seed layer was exposed. The electroplating forms were then filled with nickel (81%)-iron (19%) Permalloy using standard electroplating techniques and the nickel-iron electroplating bath described in Table I [14].

In order to insulate the bottom magnetic core from the conductor coil, polyimide was spin-coated (as above) at 4000 rpm, and hard-cured at 350°C for 1 h. Two different processes were employed to make the conductor coils, one for a deposited aluminum conductor and one for a plated conductor. For the aluminum conductor, 5 μm of aluminum was dc sputtered onto the polyimide and patterned using conventional lithography and wet etching. For the plated copper conductor, copper was plated through a thick photoresist mold. A 2000-Å-thick copper seed layer

TABLE I
COMPOSITION OF THE NICKEL-IRON AND COPPER ELECTROPLATING SOLUTIONS

Nickel-Iron Permalloy		Copper	
Component	Quantity (g/l)	Component	Quantity
$NiSO_4 \cdot 6H_2O$	200	$CuSO_4 \cdot 5H_2O$	1200 (g/l)
$FeSO_4 \cdot 7H_2O$	8	H_2O_4	100 (ml/l)
$NiCl_2 \cdot 6H_2O$	5		
H_3BO_3	25		
Saccharin	3		

was deposited, and the copper plating mold was formed in 5-μm-thick positive photoresist. The copper conductors were plated through the defined molds using standard electroplating techniques and the copper plating solution described in Table I. Upon completion of the electroplating, the photoresist was removed with acetone, and the copper seed layer was etched in an HCl-based copper etching solution.

In order to insulate the conductor line and replanarize the surface, more polyimide was deposited in multiple coats (as described above), yielding approximately 9 μm of polyimide. Via holes were then dry-etched through the polyimide layer between the meander conductors using 100% oxygen plasma and an aluminum hard mask. Upon completion of the via etch, the aluminum hard mask was removed. Electrical contact was then made to the bottom magnetic core and the vias were filled with nickel-iron using the electroplating bath and conditions described previously.

A metal sacrificial layer was then deposited and defined at the desired position of the cantilever beam. A cavity to contain the sacrificial layer was dry-etched down through the polyimide layer using an aluminum mask as described earlier, and the sacrificial layer was buried in this cavity. This approach improved the planarization of the surface for the next process. Two different metals were used as a sacrificial material: 7-μm-thick dc-sputtered Al and 7-μm-thick electroplated copper.

After an additional planarizing step, the top magnetic core and cantilever beam were plated over the magnetic vias and sacrificial layer, completing the magnetic circuit. This was achieved using an evaporated nickel seed layer defined into the desired via and beam shapes using a lift-off technique, a photoresist plating mold, and the electroplating conditions described above. Bonding pads were then opened through polyimide layers for the electrical test by using the via etch process sequence described earlier. Optionally, to remove the titanium plating seed layer located underneath the polyimide, the structure was dry-etched to the bottom, and the titanium was then selectively dry-etched using a 90% CF_4/O_2 plasma. It should be noted that removal of the magnetic core plating base was not required for successful device performance. Fig. 4(a) shows the fully fabricated device, and Fig. 6 shows a side view of the multilevel meander inductive component after this optional removal step has been carried out.

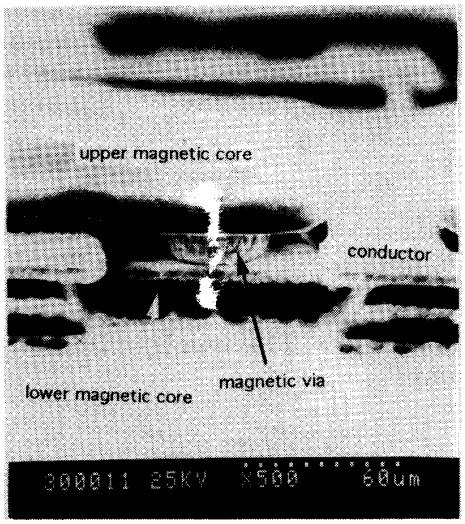

Fig. 6. Detailed side view scanning electron micrograph of a magnetic via in the MMA. A magnetic via connecting top and bottom magnetic cores along with a section of conductor is shown.

Note the magnetic via connecting the top and bottom cores in the meander topology.

Finally, the cantilever beams were released using appropriate selective etches. After release, samples were diced into chips for bonding and test.

V. ELECTROMECHANICAL MODEL

The magnetic flux that crosses an air gap in a magnetic circuit produces an attractive force between the faces of the magnetic electrodes. The magnetic core structure shown in Fig. 4 contains an air gap of variable length g as determined by the position of the movable cantilever beam. In this model, two assumptions are made: first, the magnetic flux in the air gap is distributed uniformly and thus the fringing effect is negligible; second, the permeability of the magnetic core has a constant value.

When the magnetic flux density is increased from zero to B in a magnetic circuit, the energy stored in the magnetic circuit can be expressed [15] by

$$W_\phi = (\text{vol}) \int_0^B H\, dB = (\text{vol}) \frac{B^2}{2\mu_r \mu_0}, \tag{1}$$

where (vol) is the volume of magnetic circuit, H is the magnetic field, and μ_0 and μ_r indicate the free-space and relative permeabilities respectively.

If the cantilever beam undergoes a displacement in response to the force of attraction f, the air gap is shortened by the differential length dg, and the work done by the force is given by

$$dW_{\text{mech}} = f\, dg. \tag{2}$$

If the current is adjusted so that the air gap flux remains constant while the gap is shortened by the differential distance dg, the electrical input cannot make a contribution to the energy stored in the air gap because of the constant

air-gap flux. Thus, the mechanical energy must be abstracted from the energy stored (W_ϕ) in the magnetic field while the air gap gives up the stored energy by virtue of its decreased volume, which gives

$$dW_\phi = -dW_{\text{mech}} = -\frac{A_g B_g^2}{2\mu_0} dg, \tag{3}$$

where A_g and B_g are the area and magnetic flux density of the air gap respectively.

The actual force exerted between the faces of the magnetic electrodes is obtained from (2) and (3) and can be expressed as

$$f = \frac{dW_{\text{mech}}}{dg} = \frac{A_g B_g^2}{2\mu_0}. \tag{4}$$

A scanning electron micrograph of the nickel–iron cantilever beam released from the surface and its schematic diagram with uniform load q are shown in Fig. 7. In some structures, the cantilever beam was designed to have a narrow neck near the beam support, which tended to increase the flexibility of the beam. In analyzing the bending of these cantilever beams, it was assumed that the width of the beam was equal to the width of the neck, since the deflection of the beam would be controlled by the narrow neck.

The paths of magnetic flux and the magnetic equivalent circuit for the designed magnetic microactuator can be simply drawn from the analogous structure schematic diagrams shown in Figs. 4(b) and 8(a). Analysis of the magnetic circuit in Fig. 8(a) can be facilitated by introducing the equivalent electrical circuit shown in Fig. 8(b), where the resistance R is analogous to the magnetic reluctance $\Re$, and the voltage source F denotes the magnetomotive force (mmf) Ni. From the equivalent circuits shown in parts (b) and (c) of Fig. 8, the magnetic flux ϕ_g that flows through the air gap can be obtained; consequently the magnetic flux density B_g in the air gap can be determined as

$$B_g = \frac{N_1 i \mu_0 \mu_r A_c}{0.5\ell_{c1}A_g + \ell_{c0}A_g + \mu_r A_c g}, \tag{5}$$

where, as depicted in Fig. 8(a), ℓ_{c1} and ℓ_{c0} are the core lengths, N_1 is the number of turns of conductor coil in the core length of ℓ_{c1}, A_c is the area of the magnetic core in the inductive component, and g is the initial gap spacing.

From (4), the magnetic force produced in the gap by the current i can be expressed as

$$F_{\text{mag}} = \frac{dW_\phi}{dg} = \frac{A_g}{2\mu_0}\left(\frac{N_1 i \mu_0 \mu_r A_c}{0.5\ell_{c1}A_g + \ell_{c0}A_g + \mu_r A_c g}\right)^2, \tag{6}$$

where F_{mag} is the force of magnetic origin, and μ_r is the relative permeability of the magnetic core, which is assumed to be constant (note that this assumes that the core does not saturate).

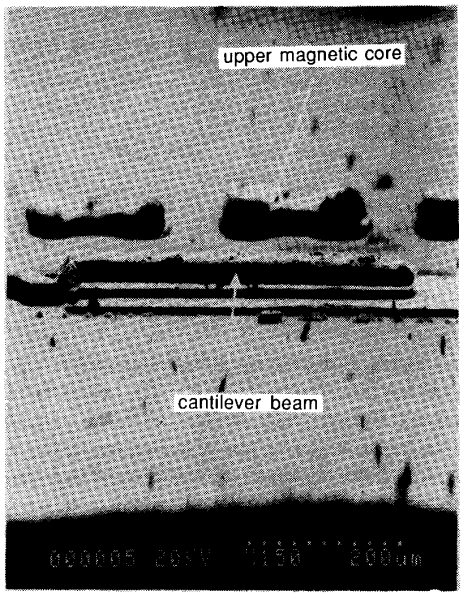

(a)

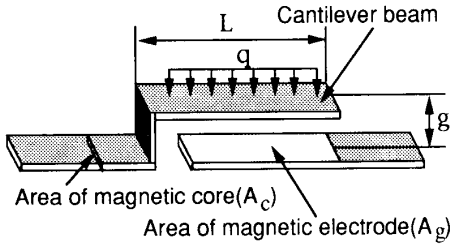

(b)

Fig. 7. Scanning electron micrograph of the nickel–iron cantilever beam released from the surface, and a corresponding schematic diagram for the electromechanical model. (a) Scanning electron micrograph of the fabricated nickel–iron cantilever beam; (b) schematic diagram for electromechanical analysis.

Since the size of the gap is small compared with the length of the beam and since the variation of magnetic reluctance along the length of the beam is small compared with the reluctance of the inductive component, the generated magnetic forces along the cantilever beam are assumed to be constant and are represented as a uniform load q along the cantilever beam in the analysis of mechanical deflection. The load–deflection relationship for a uniformly loaded cantilever beam can be expressed as [16]

$$q = \frac{8EI\,\delta_b}{L^4}, \tag{7}$$

where δ_b is the deflection of the tip of the cantilever beam, q is the distributed load along the length of the beam, E is the modulus of elasticity of the beam material, and I is the moment of inertia of the beam. Thus, by comparing (6) and (7), the relationship between the deflection of the tip of the cantilever beam and the applied current can be

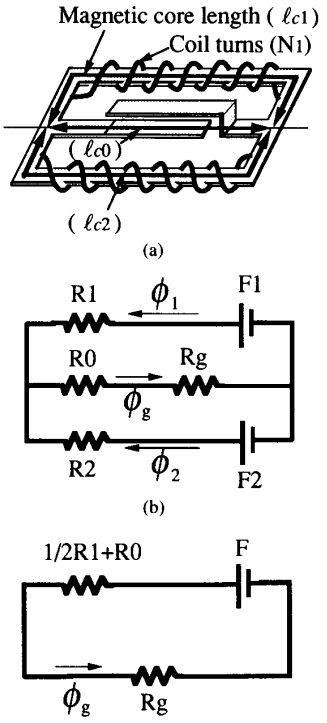

Fig. 8. Magnetic circuit model of the magnetic microactuator analogous to the equivalent electrical circuit. (a) Analogous schematic diagram of magnetic microactuator. (b) Equivalent electrical circuit, where *R0*, *R1*, *R2*, and *Rg* are the magnetic reluctance corresponding to magnetic circuit branches and air gap respectively as shown in (a). *F1* and *F2* denote the corresponding magnetomotive forces. (c) Simplified circuit, where *F* is equated to *F1* and *F2* due to magnetic circuit symmetry.

expressed as

$$\delta_b = \frac{A_g}{2\mu_0}\left(\frac{N_1 i\mu_0\mu_r A_c}{0.5\ell_{c1}A_g + \ell_{c0}A_g + \mu_r A_c g}\right)^2 \frac{L^3}{8EI}. \quad (8)$$

VI. Results and Discussion

The chip was bonded and packaged in a standard flat-pack carrier for testing. As mentioned in the fabrication, the actuators were fabricated using two different conductor materials, either the sputtered aluminum or the electroplated copper. The aluminum conductor lines showed a slightly higher conductor resistance compared with that of the copper conductor lines, in proportion to their resistivities. It was observed that the deflection of the cantilever beam was dependent almost exclusively on the amount of the applied current, independent of the conductor resistance; however, the power consumption and the device efficiency will depend on the conductor resistance. Thus, hereafter, the obtained results and the discussion are focused on the actuator fabricated with electroplated copper.

The deflection of the cantilever beam tip was measured by focusing on the tip of the deflected beam in a Nikon MM-11 Measurescope and measuring the microscope head deflection necessary to maintain focus as the beam deflected. The measured and calculated (eq. (8)) deflections of the cantilever beam as a function of applied dc current are shown in Fig. 9. As expected, the deflection is proportional to the square of current, and the measured results coincide well with the model. The available magnetic force for this microactuator is in the range of 0.1–0.8 μN. The best-fit value for the relative magnetic permeability of this material is approximately 500. This is in good agreement with measured dc magnetic relative permeabilities of 400–700, which have been measured in the linear region of test inductive structures using this material.

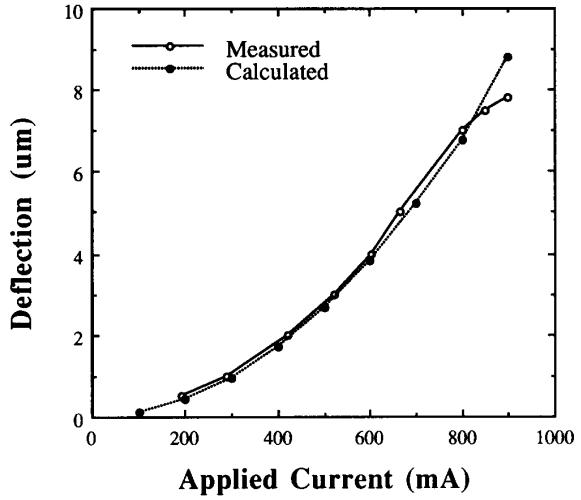

Fig. 9. The measured and calculated deflections of the cantilever beam as a function of the applied dc current.

The measured values of beam deflection in Fig. 9 begin to saturate over the current range of 850 mA, which is caused by the magnetic flux saturation in the magnetic core. From this saturation point, the saturation magnetic flux density was estimated as 0.8 (T) for the magnetic core of this magnetic actuator.

The higher the magnetic permeability that can be achieved, the better the actuator will perform. It has been reported that the permeability of plated nickel–iron magnetic material could be increased to 5000 by applying 100–500 G of magnetic field in the direction of the easy axis during the plating, and by annealing at less than 400°C with magnetic field [17]. If the permeability of the magnetic core can be improved to 2000–5000 in this structure, the magnetic forces would be in the range of several tens of μN.

One of the claimed advantages of this meander geometry is that the conductor has a relatively small resistance, since the required turns to produce a magnetic flux can be achieved in a short length of conductor without involving any conductor via connections. In comparison with a planar spiral conductor under the assumption of a constant conductor size and separation, the required length of this

meander conductor is approximately ten times shorter than that of planar spirals in achieving the same turns.

The resistance of the 17-turn meander conductor in this actuator is measured to be 1.3 Ω at 200 mA. The power consumption due to the conductor resistance at 200 mA is 52 mW. It was also observed that high current densities can be achieved in the meander conductor. For example, the maximum recommended current density of a conventional magnetic sturcture in the macro scale at 50°C has been reported as 5×10^2 A/cm^2 [18]. In the integrated magnetic microactuator, it was verified that the attainable maximum current density ranged from 5×10^4 to 5×10^5 A/cm^2, where 125 mA to 1.25 A was applied to the conductor of 50 μm × 5 μm in the size without any difficulty. These values, which are 10^2–10^3 times larger than the values in the macro scale, probably represent the large differences in surface-to-volume ratios of conductors in the macro and micro scale.

VII. Conclusions

A fully integrated surface micromachined magnetic microactuator with a meander coil and multilevel core geometry has been fabricated. Actuation has been realized by incorporating a surface micromachined nickel-iron cantilever beam as a part of the magnetic circuit of the core. Driving voltages of less than 1 V and driving currents on the order of several hundred milliamperes resulted in tip deflections of several μm, corresponding to 0.1–0.8 μN of generated magnetic force. The relatively low resistance of the meander conductor results in decreased heat dissipation in the conductor, which increases the efficiency of the device. The low drive voltages make it possible to consider integration of MMA's with IC-based control circuitry.

Acknowledgment

The authors would like to thank Y. W. Kim, A. B. Frazier, and B. Rashidian of Georgia Tech for valuable technical discussions during the course of this work. The authors would also like to gratefully acknowledge DuPont for their donations of polyimide and Lake Shore Cryotronics, Inc for their assistance in measurements of the magnetic properties of the Permalloy thin films.

References

[1] B. Wagner and W. Benecke, "Microfabricated actuator with moving permanent magnet," in *Proc. IEEE Microelectro-Mechanical Systems Workshop*, 1991, pp. 27–32.

[2] B. Wagner, M. Kreutzer, and W. Benecke, "Linear and rotational magnetic micromotors fabricated using silicon technology," in *Proc. IEEE Microelectro-Mechanical Systems Workshop*, 1992, pp. 183–189.

[3] H. Guckel *et al.*, "On the application of deep X-ray lithography with sacrificial layers to sensor and actuator construction," in *Proc. 6th Int. Conf. Solid-State Sensors and Actuators*, 1991.

[4] C. H. Ahn and M. G. Allen, "A fully integrated micromagnetic actuator with a multilevel meander magnetic core," in *Proc. IEEE Solid State Sensor and Actuator Workshop* (Hilton Head, SC), June 1992, pp. 14–18.

[5] W. S. N. Trimmer, "Microbots and mechanical systems," *Sensors and Actuators*, vol. 19, pp. 267–287, 1989.

[6] W. Benecke, "Silicon-microactuators: Activation mechanism and scaling problems," in *Proc. 6th Int. Conf. Solid-State Sensors and Actuators*, 1991, pp. 46–50.

[7] R. E. Hetrick, "A vibrating cantilever magnetic field sensor," *Sensors and Actuators*, vol. 16, pp. 197–207, 1989.

[8] R. F. Soohoo, "Magnetic thin film inductors for integrated circuit application," *IEEE Trans. Magn.*, vol. 15, no. 6, pp. 1803–1805, 1979.

[9] O. Oshiro, H. Tsujimoto, and K. Shirae, "A novel miniature planar inductor," *IEEE Trans. Magn.*, vol. 23, no. 5, pp. 3759–3761, 1987.

[10] H. M. Greenhouse, "Design of planar rectangular microelectronic inductors," *IEEE Trans. Parts, Hybrids and Packaging*, vol. 10, no. 2, pp. 101–109, 1974.

[11] S. Kawahito, Y. Sasaki and M. Ashiki, and T. Nakamura, "Micromachined solenoid for highly sensitive magnetic sensors," in *Proc. 6th Int. Conf. Solid-State Sensors and Actuators* (San Francisco), June 1991, pp. 1077–1080.

[12] R. D. MacInnis and K. V. Gow, "Tensile strength and hardness of electrodeposited nickel-iron foil," *Plating*, pp. 135–136, Feb. 1971.

[13] M. E. Henstock and E. S. Spencer-Timms, "The composition of thin electrodeposited alloy films with special reference to nickel-iron," in *Proc. 6th Int. Metal Finishing Conf.*, 1963, pp. 179–185.

[14] C. H. Ahn and M. G. Allen, "A new toroidal-meander type integrated inductor with a multilevel meander magnetic core," *IEEE Trans. Magn.*, in press

[15] L. W. Matsch, *Electromagnetic and Electromechanical Machines*. New York, IEP—A Dun-Donnelley Publisher, 1977, pp. 23–27.

[16] J. M. Gere and S. P. Timosenko, *Mechanics of Materials*. Boston, PWS-KENT Publishing, 1990, pp. 461–471.

[17] R. L. Anderson, E. E. Castellani, P. M. McCaffrey, and L. T. Romankiw, "Method for treating magnetic alloy to increase the magnetic permeability," U.S. Patent 4 003 768.

[18] C. W. T. McLyman, *Transformer and Inductor Design Handbook*. New York, Marcel Dekker, 1988, pp. 84–89.

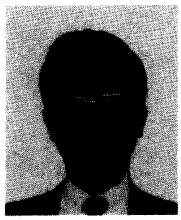

Chong H. Ahn (S'90–M'91) received the B.S. degree in electrical engineering from Inha University, South Korea, in 1980, and the M.S. degree in electrical engineering from the Seoul National University, South Korea, in 1983.

Formerly a faculty member at Inha Technical J. College, South Korea, he is currently a postdoctoral associate in the School of Electrical Engineering at the Georgia Institute of Technology, Atlanta, GA. His research interests include the development, design, fabrication, and characterization of fully integrated magnetic microsensors and microactuators, micromachined planar inductors, planar magnetic micromotors, and integrated dc/dc converters.

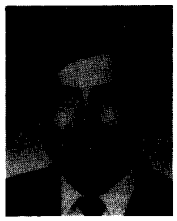

Mark G. Allen (M'89) received the B.A. degree in chemistry, the B.S.E. degree in chemical engineering, and the B.S.E. degree in electrical engineering from the University of Pennsylvania in 1984, the S.M. degree from the Massachusetts Institute of Technology in 1986, and the Ph.D. degree from MIT in 1989.

Since 1989 he has been an Assistant Professor in the School of Electrical Engineering at Georgia Institute of Technology. His research includes micromaching fabrication technology, microoptomechanical systems, and material issues in micromachined structures and electronic packages.

Dr. Allen is a member of the editorial board of the *Journal of Micromechanics and Microengineering*.